Physics and Chemistry of the Earth 64 (2013) 117–126

Contents lists available at SciVerse ScienceDirect

Physics and Chemistry of the Earth

journal homepage: www.elsevier.com/locate/pce

Thermal coupling may control mechanical stability of geothermal reservoirs during cold water injection

Silvia De Simone [a,b,*], Victor Vilarrasa [a,b], Jesús Carrera [a], Andrés Alcolea [c], Peter Meier [c]

[a] GHS, Institute of Environmental Assessment and Water Research (IDAEA), Consejo Superior de Investigaciones Científicas (CSIC), Jordi Girona 18-26, 08034 Barcelona, Spain
[b] GHS, Department of Geotechnical Engineering and Geosciences, Technical University of Catalonia (UPC-BarcelonaTech), Jordi Girona 1-3, 08034 Barcelona, Spain
[c] Geo-Energie Suisse AG, Reitergasse 11, CH-8004 Zürich, Switzerland

ARTICLE INFO

Article history:
Available online 17 January 2013

Keywords:
Hydraulic stimulation
Induced seismicity
Thermoelasticity
Elasticity in porous media
Thermo-hydro-mechanical model

ABSTRACT

Hydraulic stimulation and geothermal reservoir operation may compromise the rock mechanical stability and trigger microseismic events. The mechanisms leading to this induced seismicity are still not completely understood. It is clear that injection causes an overpressure that reduces the effective stress, bringing the system closer to failure conditions. However, rock instability may not result only from hydraulic effects, but also from thermal effects. In fact, hydro-mechanical (i.e., isothermal) models often fail to reproduce field observations because the injection of cold water into a hot reservoir induces thermal stresses due to rock contraction. Thus, rock instability is likely to result from the superposition of hydraulic and thermal effects. Here, we perform coupled thermo-hydro-mechanical and hydro-mechanical simulations to investigate the effects of cold water injection in a fracture zone-intact rock system. Results show that thermal effects induce a significant perturbation on the stress in the intact rock affected by the temperature drop. This perturbation is likely to trigger induced seismicity in the surroundings of critically oriented fractures near the injection well. Hydro-mechanical simulations show that the behavior depends on the orientation of the faults and on the initial stress tensor. In the direction of the fractures, where the strains are more constrained, total stress increases with increasing pressure; thus, deviatoric stress increases or decreases depending on the initial stress state. The comparison between hydraulic and thermal effects shows that, when the largest confining stress acts perpendicular to the fractures, thermoelastic effects dominate and could trigger induced seismicity.

1. Introduction

Geothermal energy production from deep hot rocks requires a high permeability heat exchanger for economic efficiency. The typical procedure entails intercepting natural pre-existing discontinuities, such as faults and joints, and enhancing their permeability by means of stimulation. Hydraulic stimulation is the most widely used method. It involves the massive injection of a large volume of water (several thousand cubic meters) at high flow rates to increase the downhole pore pressure, which tends to induce shearing along the fracture planes (Pearson, 1981). In this way permeability is enhanced due to dilatancy, especially in the direction perpendicular to shear (Barton et al., 1985; Yeo et al., 1998; Mallikamas and Rajaram, 2005).

Microseismic events occur during hydraulic stimulation. Induced seismicity is typically weak ($M < 2$; Evans et al., 2012) and certifies the effectiveness of the operation. However, these events are sometimes of sufficient magnitude to be felt by the local population. For example, seismic events with magnitude greater than 3 occurred at the Basel Deep Heat Mining Project in Switzerland (Häring et al., 2008) and at the Hot Dry Rock Project of Soultz-sous-Forêts in France (Cornet et al., 1997; Baria et al., 2005). This causes a negative impact on the local population and may compromise the continuation of the project. Hence, understanding the mechanisms triggering these induced micro-earthquakes is important to properly design and manage geothermal stimulation and operation so as to prevent them.

Induced seismicity occurs when failure conditions are reached, either at an existing fracture or at a newly created one. It is widely believed that the main cause of failure during hydraulic stimulation is overpressure (Shapiro et al., 1999, 2003; Parotidis et al., 2004). Indeed, overpressure produces a reduction of effective stresses that can cause the fracture to yield. Rutqvist and Stephansson (2003) provide an accurate review of the hydro-mechanical coupling in fractured rock and point out its relevance in the geothermal field. However, pore pressure cannot be considered the only cause of induced seismicity. Microseismic events at Soultz-sous-Forêts (Baisch et al., 2010; Evans et al., 2005) and Basel (Häring et al.,

* Corresponding author at: GHS, Institute of Environmental Assessment and Water Research (IDAEA), Consejo Superior de Investigaciones Científicas (CSIC), Jordi Girona 18-26, 08034 Barcelona, Spain. Tel.: +34 665737253.
E-mail address: silviadesi@gmail.com (S. De Simone).

1474-7065/$ - see front matter © 2013 Elsevier Ltd. All rights reserved.
http://dx.doi.org/10.1016/j.pce.2013.01.001

2008; Ripperger et al., 2009) were still occurring once injection stopped and often the largest microseisms occurred after the end of injection, like in Basel. These post injection events cannot be explained by pressure diffusion alone, because its magnitude decreases quickly with time (Delleur, 1999).

Interestingly, injected water was cold both at Basel and Soultz. The temperature contrast between the hot reservoir and the injected water (at atmospheric conditions at surface) was large. This produces a significant contraction of both the fracture filling and the surrounding rock, leading to an additional reduction in effective stresses, which has to be taken into account (Majer et al., 2007). This effect is confirmed by the measurements taken at the Geysers geothermal steam field (Santa Rosa, California), where the observed seismicity is not directly related to overpressure (National Research Council, 2012). There, the large temperature difference between the injected fluid and the deep rock produced a significant cooling of the geothermal reservoir (Mossop and Segall, 1997), which caused thermal contractions of the rock, affecting the in situ stress state. In short, thermal effects should be considered to better understand the processes involved in geothermal reservoir stimulation (Segall and Fitzgerald, 1998). To achieve this, coupled thermo-hydro-mechanical analyses are necessary.

Thermoelastic effects in geothermal systems have been studied by some authors (e.g. Ghassemi, 2012). They performed thermo-hydro-mechanical models of cold water injection into a planar fracture (Kohl et al., 1995; Ghassemi et al., 2007, 2008; Ghassemi and Zhou, 2011) or in a fracture network (Kolditz and Clauser, 1998; Bruel, 2002; McDermott et al., 2006). Nevertheless, most of them solely point out the perturbations generated within the fracture or at the fracture's surface, but not the effects on the surrounding rock mass.

We conjecture that the thermal effects developing in the cooled part of the rock matrix may play an important role in triggering induced seismicity. In fact, the intact rock has a greater stiffness than the fracture, so that thermal stress changes may indeed be large, which could explain how seismic events are triggered. To investigate this, we simulate the hydraulic stimulation of an idealized fracture zone embedded in an intact rock matrix. Hydraulic and thermal effects are studied by means of fully coupled thermo-hydro-mechanical (THM) simulations of cold water injection into the hot fracture zone/matrix system. The results of the THM simulation are compared to those of a hydro-mechanical (HM) simulation (i.e. injection of water in isothermal equilibrium with the hot rock) in order to estimate the impact of the thermal effects.

2. Methods

2.1. Conceptual model

To investigate the effect of the cooling front caused by cold water injection on thermoelastic strain, we perform coupled HM and THM numerical simulations of water injection into a rock mass containing a zone of discontinuities. An idealized geometry consisting of a planar fracture zone (corresponding to joints or faults) of 1 m thickness embedded into an intact rock mass is considered. The fracture zone is treated like a continuous porous medium. This assumption is made considering that faults often consist of a fault core with a thickness of few centimeters embedded into a highly damaged zone of some tens of centimeters (Gudmundsson, 2004; Cappa and Rutqvist, 2011). The whole fracture zone is surrounded by the host rock, which is generally less permeable and stiffer than the fracture zone. In fractured crystalline rocks the intrinsic permeability of the intact rock matrix may be some 5 orders of magnitude smaller than that of the fault zone (Rutqvist and Stephansson, 2003). This difference in hydraulic properties converts the fault zone into a preferential flow path.

The numerical simulations calculate deformations and changes in the stress field due to cold water injection. Linear elasticity is assumed for the whole model. In order to evaluate the potential induced seismicity, we perform a slip tendency analysis (Byerlee, 1978; Morris et al., 1996; Streit and Hillis, 2004). We consider the Mohr–Coulomb failure criterion (Jaeger et al., 2007)

$$\tau_r = c + \mu \cdot \sigma'_n \tag{1}$$

where τ_r is the critical shear stress, c is cohesion, σ'_n is effective normal stress and μ is friction coefficient, which is often expressed in term of the angle of friction ϕ ($\mu = \tan\phi$).

For cohesion-less materials ($c = 0$), sliding occurs when the shear stress τ equals the critical shear stress τ_r, i.e. when the ratio of the shear stress to effective normal stress equals the friction coefficient μ

$$\frac{\tau}{\sigma'_n} = \tan\phi \tag{2}$$

We use this equation to estimate the mobilized friction angle ϕ_{mob} on critically oriented planes (i.e. the one for which ϕ_{mob} is maximum). This value quantifies the shear slip tendency along a plane, because it represents how close is the stress state to the failure envelope.

2.2. Mathematical model

According to linear theory of poro-thermoelasticity (McTigue, 1986), stresses are a function of strain, fluid pressure and temperature

$$\Delta\boldsymbol{\sigma} = K\varepsilon_v\mathbf{I} + 2G\left(\boldsymbol{\varepsilon} - \frac{\varepsilon_v}{3}\mathbf{I} + \frac{1}{2G}\Delta p_f\mathbf{I} - \frac{3K}{2G}\alpha_T\Delta T\mathbf{I}\right) \tag{3}$$

where $\boldsymbol{\sigma}$ is the total stress tensor, ε_v is volumetric strain, $\mathbf{I}$ is the identity matrix, $\boldsymbol{\varepsilon}$ is the strain tensor, $K = E/(3(1-2\nu))$ is the bulk modulus, $G = E/(2(1+\nu))$ is the shear modulus, E is the Young's modulus, ν is Poisson ratio, p_f is the fluid pressure, α_T is the linear thermal expansion coefficient and T is temperature. Biot coefficient has been assumed to be 1 because the rock compressibility is negligible compared to that of the grains. Moreover, this value is the least favorable, because it leads to the strongest hydromechanical coupling (see also Zimmerman, 2000). Notice that a temperature drop implies an isotropic drop in stresses equal to $3K\alpha_T\Delta T$, which can be very large for stiff rocks.

To solve the mechanical problem, the momentum balance has to be satisfied. If the inertial terms are neglected, it reduces to the equilibrium of stresses

$$\nabla\cdot\boldsymbol{\sigma} + \mathbf{b} = \mathbf{0} \tag{4}$$

where $\mathbf{b}$ is the vector of body forces.

Eq. (3) is coupled with the flow equation through fluid pressure. Assuming that there is no external loading and neglecting solid phase compressibility, fluid mass conservation of the fluid can be written as

$$\frac{\phi}{K_f}\frac{\partial p_f}{\partial t} + \nabla\cdot\frac{d\mathbf{u}}{dt} + \frac{1}{\rho}\nabla\cdot(\rho\mathbf{q}) = f_w \tag{5}$$

where ϕ is porosity, $1/K_f$ is water compressibility, t is time, $\mathbf{u}$ is the solid displacement vector, $\mathbf{q}$ is the water flux and f_w is an external supply of water. Notice that the second term represents the rate of change in volumetric strain (i.e. porosity). The water flux is given by Darcy's Law

$$\mathbf{q} = -\frac{k}{\mu(p_f,T)}(\nabla p_f + \rho(p_f,T)\cdot g\cdot\nabla z) \tag{6}$$

where k is the intrinsic permeability, g is gravity, z is the vertical coordinate, and μ and ρ are respectively the fluid viscosity and

density, which are function of pressure and temperature. Note that the flow equation (Eq. (5)) is coupled to the mechanical equation (Eq. (3)) through the volumetric strain (second term in the left-hand side of Eq. (5)), which can be expressed as the divergence of the displacement vector.

An additional equation governing energy balance must be accounted for thermo-hydro-mechanical coupling,

$$\frac{\partial(c_s\rho_s(1-\phi)T+c_f\rho\phi T)}{\partial t}+\nabla\cdot\left(-\lambda\nabla T+c_f\rho T\mathbf{q}+c_f\rho\phi T\frac{d\mathbf{u}}{dt}+c_s\rho_s(1-\phi)T\frac{d\mathbf{u}}{dt}\right)=f_Q \quad (7)$$

where c_s and c_f are the specific heat capacity of the solid and the fluid, respectively, ρ_s is the solid density, λ is the equivalent thermal conductivity and f_Q is an external/internal supply of energy.

Eqs. (3), (5), (6), and (7) show the strong coupling of the problem (Zimmerman, 2000). Water pressure influences stresses and strains and it is in turn influenced by the latter, which also change porosity and thus intrinsic permeability. Temperature variations affect stresses directly (see Eq. (3)), but also indirectly because water flux depends on temperature by means of density and viscosity. Temperature variation is also affected by water flux because it affects the advective transport of energy.

2.3. Numerical model

Simulations are carried out with the finite element numerical code CODE_BRIGHT (Olivella et al., 1994, 1996) that solves coupled thermo-hydro-mechanical problems in porous media.

The model domain consists of a homogeneous radial horizontal 1 m-thick fracture zone underlain and overlaid by a 250 m-thick low-permeability matrix. We model a 2D vertical section of the formation making use of the axisymmetry around the vertical well axis. The top of the fracture zone is located at a depth of 4250 m.

Table 1
Properties of the fracture zone and the intact matrix.

Parameters	Fracture zone	Matrix	Units
Intrinsic permeability	10^{-13}	10^{-18}	m^2
Porosity	0.5	0.01	
Young's modulus	100	10,000	MPa
Poisson ratio	0.3	0.3	
Thermal conductivity	2.5	1.5	$W\,m^{-1}\,K^{-1}$
Longitudinal dispersivity for heat	1	1	m
Transverse dispersivity for heat	0.1	0.1	m
Linear thermal expansion coefficient	1×10^{-5}	1×10^{-5}	$°C^{-1}$
Specific heat for solid phase	800	800	$J\,kg^{-1}\,K^{-1}$

The lateral extension is 2000 m, which ensures that pressure and thermal perturbations are contained inside the modeled domain and are not affected by spurious boundary effects.

The fracture zone is softer than the intact matrix. The value of the Young's modulus for the intact rock matrix is assumed to be 10,000 MPa, typical of crystalline rock (Goodman, 1989; Hoek, 2006). In fault zones the stiffness is usually lower (Schultz, 1996; Gudmundsson, 2004; Faulkner et al., 2006) and can vary largely depending on alteration. Due to this uncertainty, a very low value of 100 MPa is considered and a sensitivity analysis is performed. For simplicity both the fracture zone and the fractures contained in the intact rock are considered cohesion-less. The parameters assumed for the simulations are shown in Table 1 (values of intrinsic permeability and thermal conductivity are considered constant during the simulations for simplicity).

Initial conditions correspond to hydrostatic pressure, a geothermal gradient of 33 °C/km with a surface temperature of 5 °C (i.e., 150 °C at the fracture zone) and lithostatic vertical stress. The stress regime is considered axisymmetric with the vertical stress greater than the horizontal stresses following the relationship $\sigma'_h = 0.5\sigma'_v$. Conditions of constant pressure and temperature are imposed at the outer boundary of the model, whereas no flow conditions are adopted for the other boundaries. The mechanical boundary conditions are the lithostatic stress on the upper boundary and in the other boundaries no displacement perpendicular to them. Initial and boundary conditions and a schematic representation of the geometry are shown in Fig. 1.

Water is injected in the fracture zone with a mass flow rate of 3 kg/s, uniformly distributed along the contact between the fracture zone and the well, which has a radius of 0.5 m. Water injection lasts for 10 days. Unless the opposite is explicitly stated, all figures displayed hereon contain results at this time. In the THM simulation the temperature of the injected water is assumed to be 60 °C.

A structured mesh with 8925 structured quadrilateral elements is used. The mesh is refined in the areas affected by the perturbations. In order to obtain a good accuracy of the results without using a huge number of elements, the element size is smaller close to the injection well, in the fracture zone and its surroundings and increases progressively, varying from a minimum of about $8\times10^{-2}\,m^2$ next to the injection well in the fracture zone to a maximum of $700\,m^2$ close to the outer boundary.

3. Results

3.1. HM and THM coupling

Water injection produces an increase in fluid pressure, which extends further in the fracture zone than in the matrix due to the large contrast in hydraulic conductivity between the materials (Fig. 2b). After 10 days of injection, overpressure (increase of

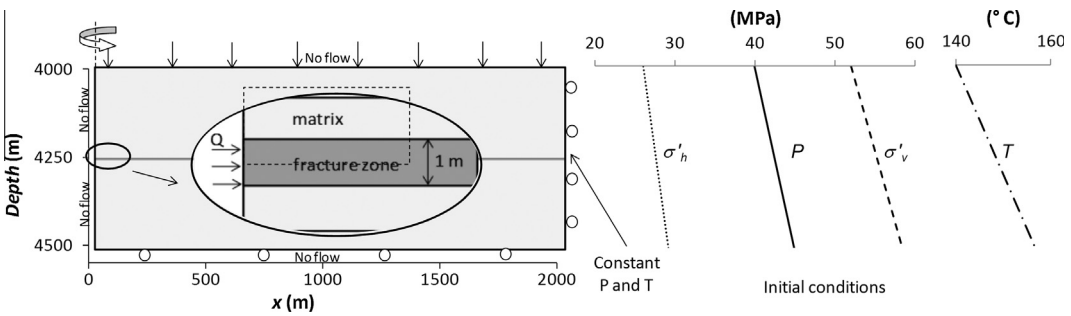

Fig. 1. Model geometry, boundary and initial conditions – liquid pressure (solid line), horizontal (dotted line) and vertical (dashed line) effective stress, temperature (dot-dashed line) vs depth. The dashed box indicates the location of the reference area shown in Fig. 2.

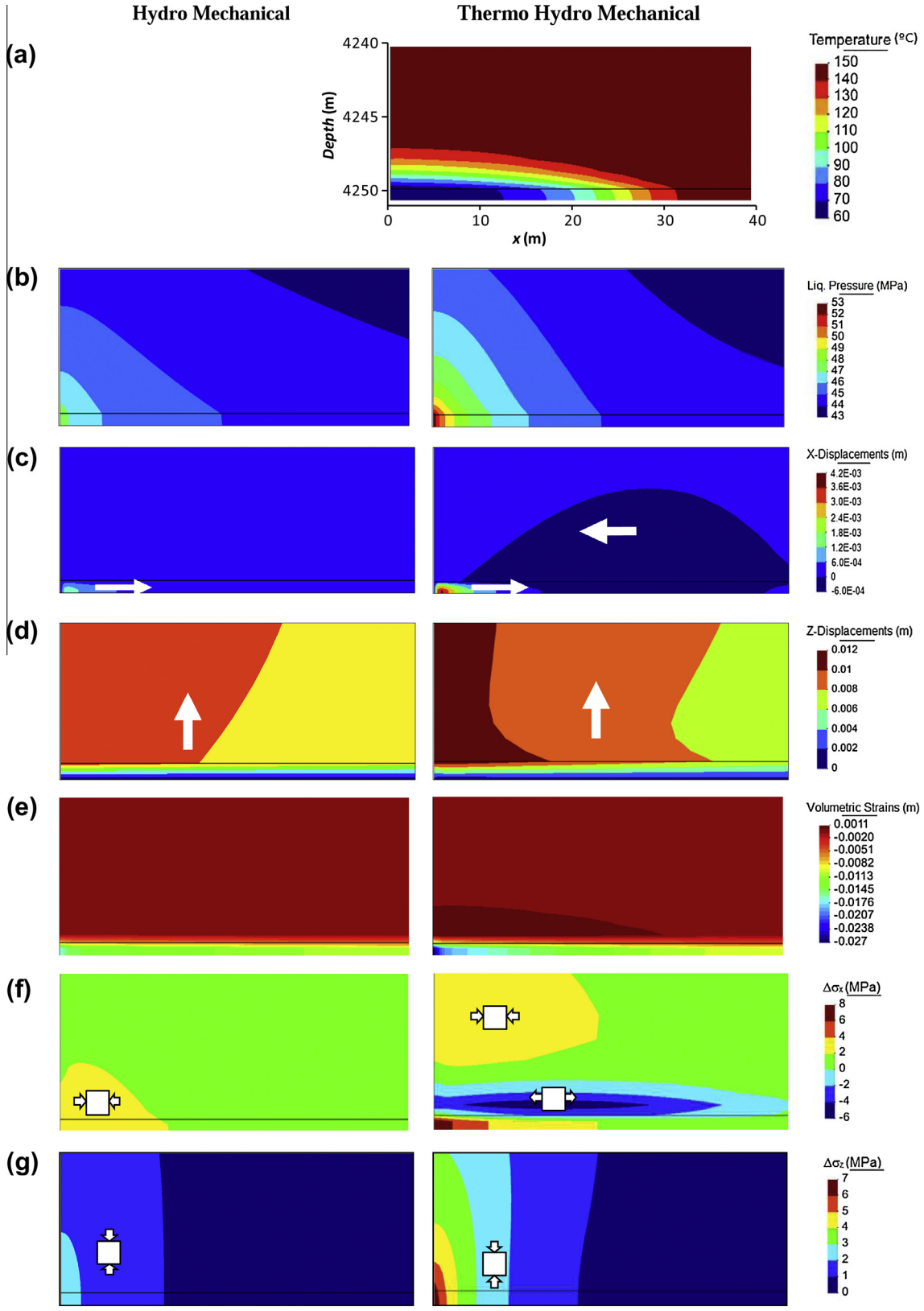

Fig. 2. Distribution of temperature (a), liquid pressure (b), horizontal (c) and vertical displacements (d), volumetric strains (e), total horizontal (f) and vertical stresses variations (g) for cold water injection and injection of water in thermal equilibrium with the formation in the reference area (recall Fig. 1). The sign criterion for deformation in (e) is that positive volumetric strain indicates contraction and negative volumetric strain means expansion. Positive displacements (c and d) are oriented as the corresponding axis.

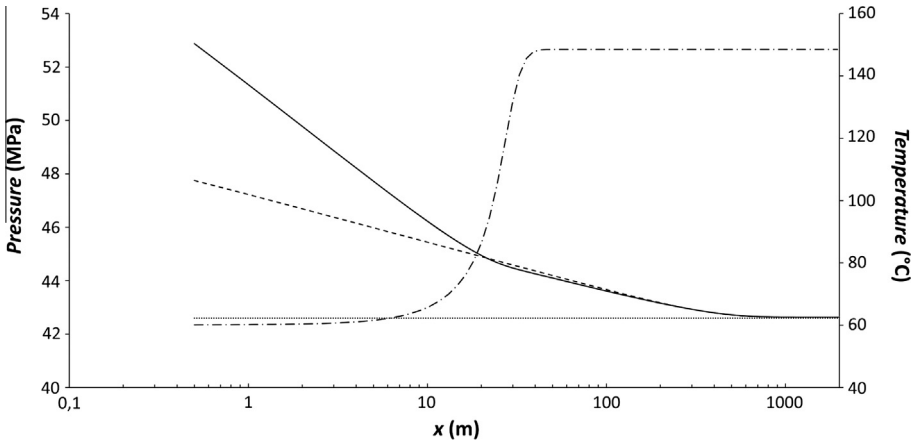

Fig. 3. Liquid pressure (dashed line HM, solid line THM) and temperature (dot-dashed line) vs distance inside the fracture zone after 10 days of water injection. The dotted line indicates the undisturbed liquid pressure.

pressure with respect to the initial value) propagates several hundreds of meters within the fracture zone (Fig. 3), but only a few meters into the matrix.

Temperature propagates much slower than overpressure along the fracture zone (Fig. 2a). After 10 days of cold water injection, the cooling front propagates within the first 20 m of the fracture zone in the longitudinal direction and penetrates 1 m into the matrix in the transverse direction (Fig. 2a). Heat transport in the fracture zone is the result of combined advection and conduction, whereas it is mainly governed by conduction in the matrix, where water flow is negligible.

The temperature reduction increases fluid viscosity, thus decreasing hydraulic conductivity. As a result, injection of cold water produces a larger overpressure than injection of warm water (Fig. 3). With the given conditions, the resulting overpressure close to the well is almost twice in the THM simulation than in the HM simulation (Figs. 2b and 3). The decrease of overpressure with the logarithm of distance from the well, which should be linear for a homogeneous medium, exhibits two different slopes for HM and THM simulation in the first 20 m, because of the temperature difference. Note that, in reality, the decrease in hydraulic conductivity caused by the increase in viscosity of the injected cooler water may be more than compensated by the increase caused by thermal contraction of the matrix, which tends to open the fracture zone, thus increasing its permeability. This effect has not been simulated in this model, as we consider constant permeability.

Effective stresses decrease as water pressure increases. As a consequence, the whole medium deforms, with greater strains in the vertical direction than in the horizontal one, due to the horizontal orientation of the fracture zone (Fig. 2c and d). Water injection compresses the fracture zone causing horizontal displacements directed away from the well. The overpressure expands the

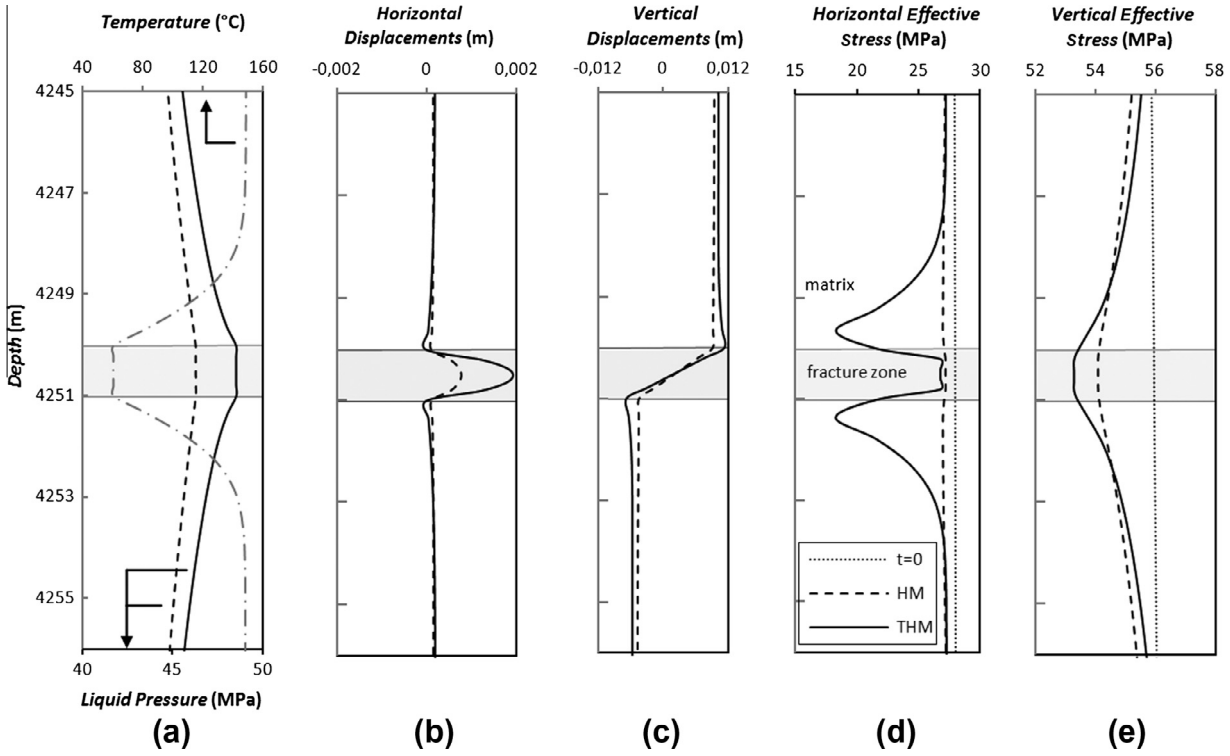

Fig. 4. Vertical profile of liquid pressure and temperature (a), horizontal (b) and vertical (c) displacements, horizontal (d) and vertical (e) effective stresses for a section placed 3 m away from the well. The solid line represent the THM solution, the dashed line represents the HM solution and the dotted line the initial situation.

fracture zone in the vertical direction causing displacements directed upwards in the upper side and downwards in the lower side, which tends to open it. This hydraulic effect is superimposed in the THM simulation to the thermal perturbation that contracts the rock as it cools. Fig. 4 displays the vertical and horizontal displacements as a function of depth for a section placed 3 m away from the injection well. The fracture zone expands as a result of overpressure in both HM and THM simulations. Indeed, the expansion in the fracture zone is larger when thermal effects are accounted for because the overpressure is larger than in the isothermal case (Fig. 4a). However, in the THM simulation, the cooled portion of the matrix undergoes a thermal contraction (see Fig. 2e), which leads to an increased opening of the fracture zone (i.e., larger vertical displacement in Fig. 4c).

Fig. 4d and e displays the variations of effective stresses due to pressure and temperature perturbations. In the HM simulation, the overpressure and the stress perturbation affect mainly the fracture zone because water flow in the matrix is negligible. Vertical effective stresses decrease more than the horizontal effective stresses because the fracture zone can deform more significantly in the vertical direction than in the horizontal direction. This behavior is also observed in the THM simulation, but with a greater effective stress reduction due to the greater overpressure. However, the most relevant effects of the THM coupling concern the region of the matrix affected by the temperature drop. Here the stress reduction due to thermal effects is much greater than in the fracture zone because of its higher stiffness (recall Eq. (3)). Additionally, the horizontal effective stress reduces more than the vertical one, leading to an increase in deviatoric stress.

3.2. Rock stability and potential induced seismicity

We represent the stress state by means of the Mohr circles. Fig. 5 displays the stress state for points placed 3 m away from the well at different depths: inside the fracture (point A), at the contact between the fracture and the matrix (point B) and inside the matrix at 0.4 m from the contact (point C). Results of the HM simulation show that the vertical effective stress decreases more than the horizontal one. This produces a reduction of the size of the Mohr circle for all points. In the case of THM simulation, the thermal contraction causes an increase of the deviatoric stress in the cooled section of the matrix. This results in a bigger Mohr circle for points B and C. Note that the Mohr circle size is greater in the latter point, reflecting a more critical situation. Inside the fracture zone (point A) the results of THM and HM simulation are similar and depict a more stable condition.

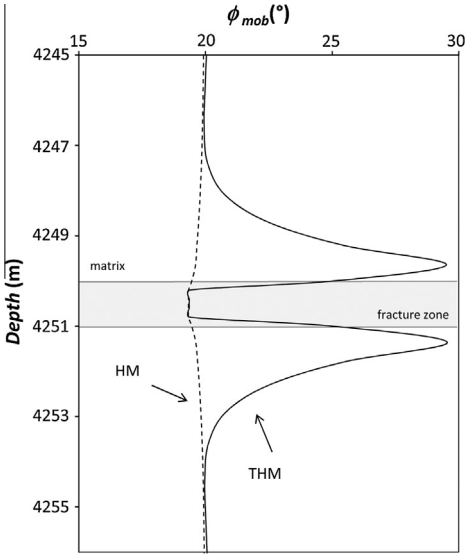

Fig. 6. Vertical profile of the mobilized friction angle for a section placed 3 m away from the injection well. Dashed line represents HM simulation and solid line represents THM simulation.

According to the Mohr circles, in the fracture zone and its surroundings the mobilized friction angle decreases in the HM simulation (Fig. 6). As the mobilized friction angle expresses the proximity to failure conditions, this reduction points to a more stable situation, which is consistent with the fact that we are assuming a normal initial stress tensor (vertical stress larger that horizontal stresses). Under these conditions, opening tends to concentrate on vertical fractures. On the other hand, in the THM simulation significantly higher friction angles are mobilized in the portion of matrix close to the fracture. However, the mobilized friction angle becomes smaller than the original one (that is about 19°) in the central part of the fracture zone. Here, thermal effects have little influence because hydraulic effects dominate (Fig. 7).

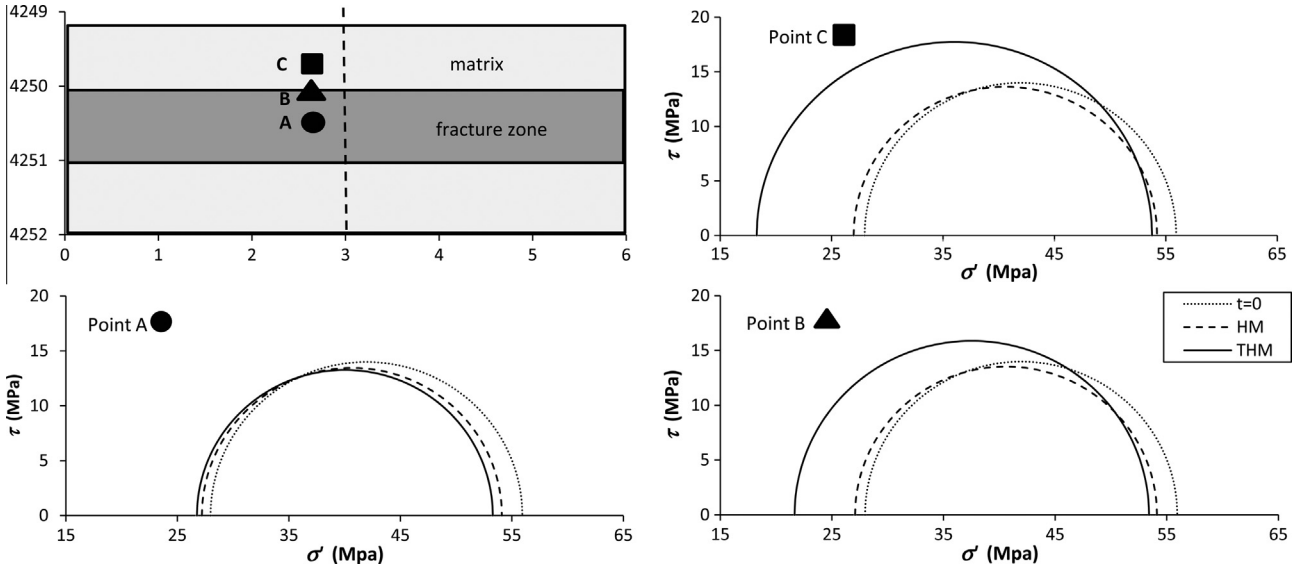

Fig. 5. Stress field after 10 days of injection for points placed 3 m away from the injection well at different depths. The solid line represent the THM solution, the dashed line represents the HM solution and the dotted line the initial situation.

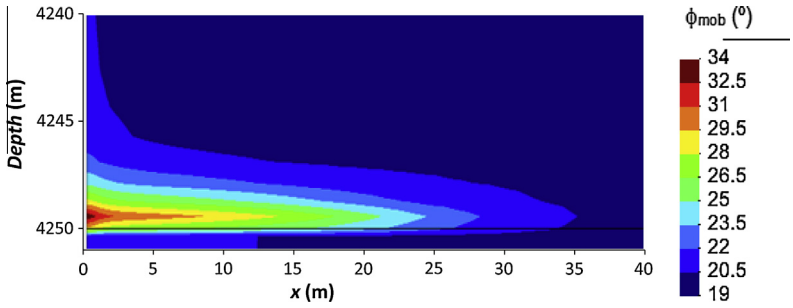

Fig. 7. Distribution of the mobilized friction angle in the reference area for THM simulation. The mobilized friction angle quantifies the shear slip tendency along critically oriented planes. The area in the intact rock matrix close to the injection well results to be the most critical for slip potential and induced seismicity.

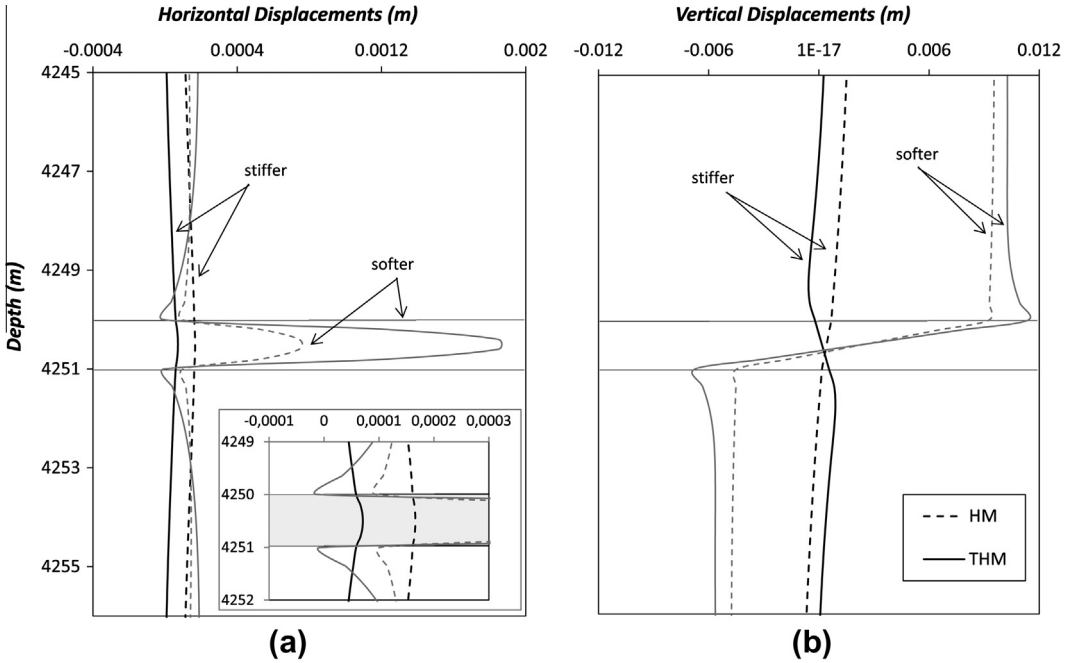

Fig. 8. Sensitivity to the stiffness of the fracture zone. Vertical profile of horizontal (a) and vertical (b) displacements for a section placed 3 m away from the well. The results of a stiffer fracture zone (E = 5000 MPa) are in black and for a softer fracture zone (E = 100 MPa) are in gray. The dashed lines represent the HM simulation and the solid lines the THM simulation. Fig. 8a contains an enlargement of the horizontal displacements in the fracture zone.

3.3. Sensitivity analysis

3.3.1. Sensitivity to stiffness of the fracture zone

We investigate the effects of the fracture zone's stiffness on the HM and THM simulations. Young's modulus is increased from 100 to 5000 MPa. As expected, the increase in stiffness leads to a significant reduction of horizontal and vertical displacements in the HM simulations (Fig. 8). In the THM simulation this behavior is superimposed to the thermal contraction, which further reduces the displacements to the point that vertical displacements even become negative within the fracture zone. That is, thermal effects dominate hydraulic effects.

Lower rock compressibility yields smaller storage coefficients. This results in slightly higher overpressures, because the hydraulic response to fluid injection is faster. This fact provokes a greater reduction in effective stresses (in both the HM and THM simulations) with respect to the simulation with a softer fracture zone (Fig. 9a and b). However, the most relevant sensitivity to the stiffness of the fracture zone concerns the thermal perturbation of the effective stresses. Indeed, according to Eq. (3), the thermal stress is proportional to the Young's modulus. As a consequence, thermal stresses become significant also in the fracture zone when it is stiffer. Thus, a stiffer fracture zone reduces stability and yields a higher mobilized friction angle (see Fig. 9c) in the fracture and in the fracture-matrix contact when cold water is injected.

3.3.2. Sensitivity to initial stress condition

Sensitivity to initial stress condition is investigated taking into account a reverse faulting stress regime, in which the maximum principal stress is horizontal, with a lateral earth pressure coefficient of 2, i.e. $\sigma'_h = 2 \cdot \sigma'_v$. The change of the initial stress field evidently does not affect the net variation of effective stresses, which are the same as in the normal faulting stress regime. Nevertheless, since now the maximum principal stress is horizontal, the effective stress perturbation results in an increase of the size of the Mohr circle in the HM simulation and a decrease in the THM simulation.

This leads to an opposite behavior with respect to the normal faulting stress regime: the mobilized friction angle in the matrix increases for isothermal injection and decreases for cold water injection (Fig. 10), but with a smaller magnitude because of the greater confining stresses.

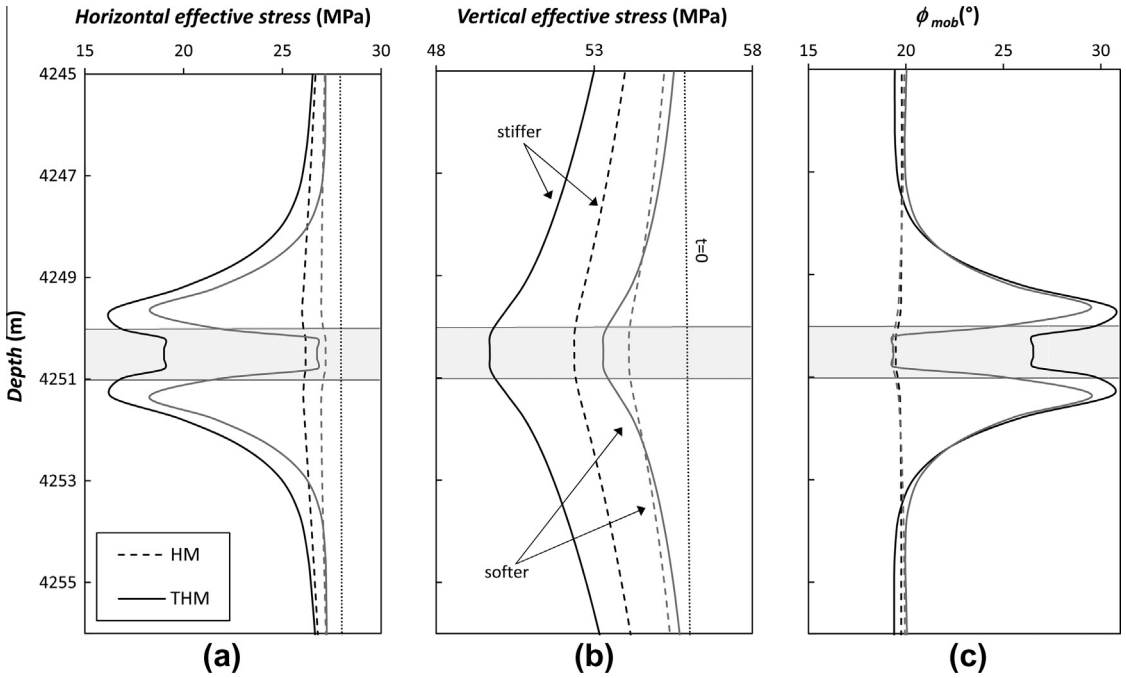

Fig. 9. Sensitivity to the stiffness of the fracture zone. Vertical profile of horizontal (a) and vertical (b) effective stresses and of mobilized friction angle (c) for a section placed 3 m away from the well. The results of a stiffer fracture zone (E = 5000 MPa) are in black and for a softer fracture zone (E = 100 MPa) are in gray. The dashed lines represent the HM simulation, the solid lines the THM simulation and the dotted lines represent the initial situation.

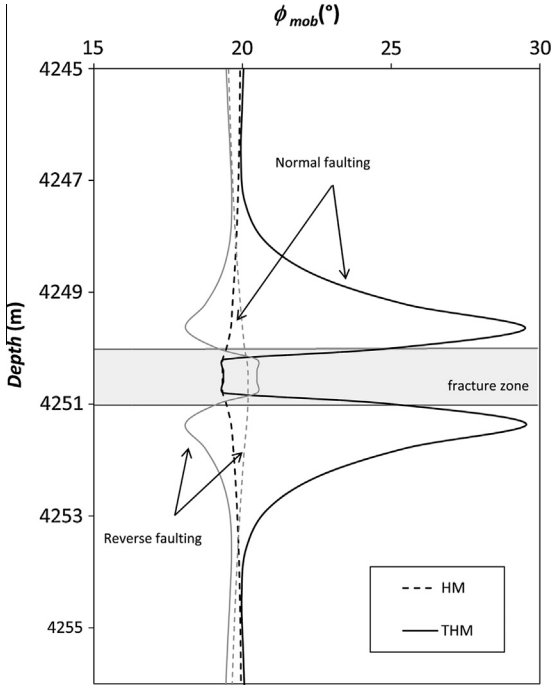

Fig. 10. Sensitivity to initial stress conditions. Vertical profile of mobilized friction angle for a section placed 3 m away from the well. In black are the results for normal faulting stress regime and in gray for reverse faulting stress regime. Dashed lines represent the HM simulation and solid lines the THM simulation.

4. Discussion

Water injection produces an overpressure that reduces effective stresses and tends to open fractures. Even though overpressure acts isotropically and tends to expand the medium in all directions, confinement restricts expansion strains and implies an increase of total stresses, especially in the plane of the fracture. Thus, the decrease of effective stresses is smaller than the increase in fluid pressure (Engelder and Fischer, 1994; Hillis, 2000). This effect is not predicted by uncoupled models that simply apply the variation of pore pressure on the effective stress state. In the case discussed here (a horizontal fracture zone) the fracture zone can deform more in the vertical direction than in the horizontal one (Fig. 4b and c), due to the geometry and the confinement conditions. This implies a greater increase in horizontal total stress than in vertical total stress (Fig. 2f and g). As a result, the effective stress decreases more in the vertical than in the horizontal direction (Fig. 4d and e). This means that the deviatoric stress decreases with increasing pressure. Therefore, under isothermal conditions, even though the Mohr circle displaces to the left, which causes instability, its size may also be reduced (Vilarrasa et al., 2010), which partly compensates this instability (Fig. 5). This behavior explains the induced seismicity observed in depletion processes, such as oil and gas extraction (Segall et al., 1994; Ferronato et al., 2008). In these processes the opposite occurs, i.e. deviatoric stress increases for decreasing pressure.

Acknowledging thermal effects leads to two main differences with respect to the isothermal case. First, cold water injection produces a higher overpressure because water viscosity increases for decreasing temperatures (Figs. 3 and 4a). This results in a larger effective stress reduction and larger expansion strains than in HM simulations. Second, cold water also contracts the rock, causing a decrease of both total and effective stress. The magnitude of the thermal stress is proportional to the temperature drop and to the stiffness of the material (Eq. (3)). Therefore, the thermal stresses reduction is much greater in the matrix than in the fracture zone. The net result is that the fracture zone is mainly affected by overpressure, which produces effects comparable to those of the isothermal case (Figs. 4d and e, 5 and 6). In contrast, the rock matrix undergoes greater thermal than hydraulic perturbations. In particular, the horizontal stress decreases more than the vertical

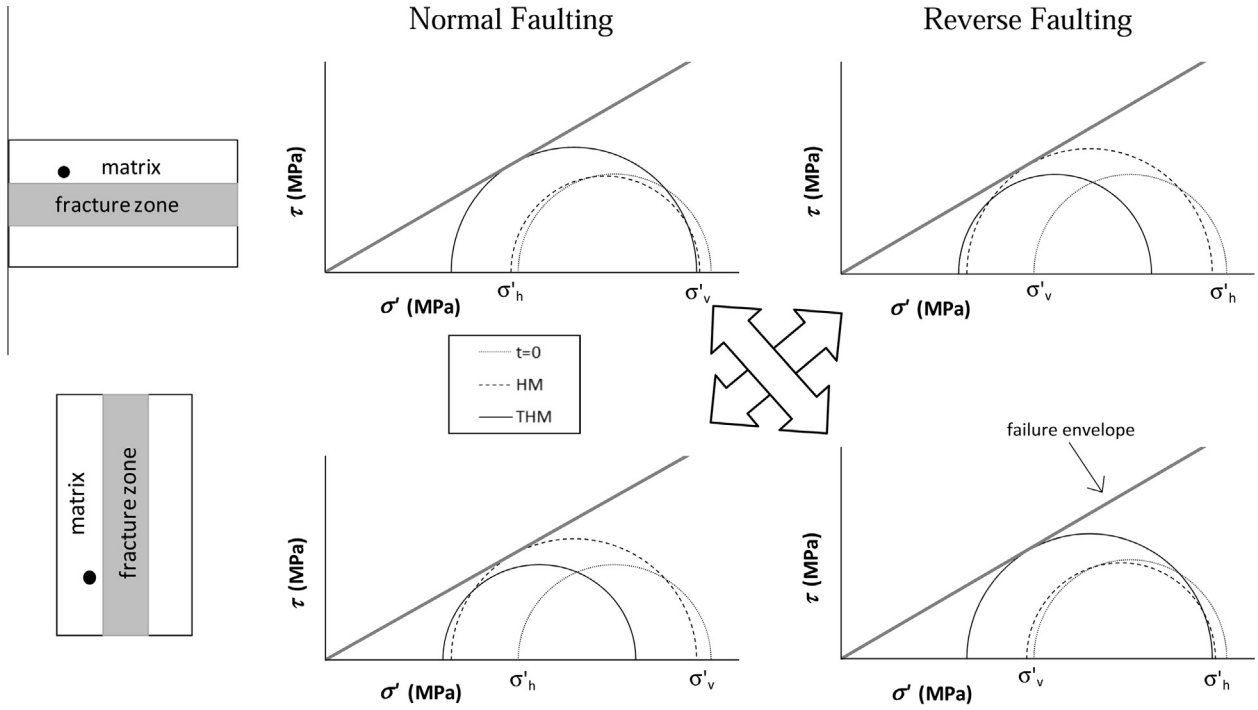

Fig. 11. Schematic description of the stress state changes in the case of horizontally and vertically oriented fracture zone under different stress regimes (for a point placed in the matrix close to the fracture zone). The solid line represents the THM solution, the dashed line represents the HM solution, the dotted gray line the initial situation and the straight thick line represents the failure envelope.

one (Fig. 4d and e). This difference is due to the relatively large horizontal extent of the temperature perturbation and its limited vertical extent. In fact, in the horizontal direction the cooled zone extends about 20 m, while in the vertical directions extends only a few meters. This provokes horizontal thermal stresses much greater than the vertical ones. As a result, in the cooled portion of the matrix (points B and C) the deviatoric stress and the Mohr circle's size increase (Fig. 5), denoting unstable conditions (Fig. 6). Note that the mobilized friction angle reaches value of 34° close to the well (Fig. 7), which would induce a microseism if a reasonable friction angle of about 30° is assumed (Zoback, 2007).

Actual stability conditions depend on the initial stress regime. When the maximum principal stress is horizontal (i.e., reverse faulting regime), the deviatoric stress increases for isothermal water injection and decreases for cold water injection in a horizontal fracture. Therefore, the most unfavorable conditions occur for isothermal injection and reverse faulting stress regime or for cold water injection and normal faulting stress regime (Fig. 10).

It is worth noting that the described phenomenon is valid for any orientation of the fracture zone. We built up and performed models considering the same configurations but with a vertical orientation of the fracture zone. The models confirm that the orientation has little influence on the general behavior. When we account for HM coupling, the decrease in effective stress caused by fluid injection is always smaller than overpressure and largest in the direction perpendicular to the fracture zone. On the other hand, when thermal perturbations are considered, the greatest effective stress reduction occurs in the direction of the fracture zone. In short, a vertically oriented fracture zone with reverse faulting stress regime acts in the same way than a horizontally oriented one with normal faulting stress regime (Fig. 11). Thus, when cold water is injected the critical situation is likely to take place when the greater stress acts normal to the fractures. This is the scenario of Basel and Soultz-sous-Forêts, where strike slip faulting ($\sigma_H > \sigma_v > \sigma_h$; where σ_H and σ_h are respectively the maximum and the minimum principal horizontal stresses and σ_v is the vertical stress) is present and therefore shear slip occurs preferentially on vertical or sub-vertical fractures.

The hydro-mechanical and thermo-mechanical effects are very sensitive to the problem settings, i.e. stiffness and thickness of the fracture zone. What is clear is that the temperature drop leads to an unstable situation in the surrounding rock mass. This could eventually induce microseismicity in critically oriented fractures that are close to failure. Nevertheless, these thermal effects are relatively local (some 20 m for the conditions tested in this work) and cannot explain the seismic events with epicenters tens or hundreds of meters far from the injection point. It could be conjectured that these far events are provoked by a cascade effect (Häring et al., 2008). Testing this conjecture requires non-linear simulations, which are planned as future work.

It should be lastly underscored that hydro-mechanical and thermo-mechanical processes occur with different response times. Once the injection stops, the hydro-mechanical perturbation will quickly disappear, while the cooling front will continue to penetrate slowly into the rock mass. In this way thermal contribution to deformations and stress perturbation will last after the cessation of injection and can represent a triggering factor of the delayed seismic events (Ghassemi et al., 2007). The analysis discussed here is restricted to the stimulation period. Further work will include simulation of the post injection period.

5. Conclusions

We have performed thermo-hydro-mechanical models to investigate the effects of cold water injection in a geothermal reservoir. The model considers a fracture zone embedded into a rock matrix. We perform and compare coupled thermo-hydro-mechanical and hydro-mechanical simulations. This approach facilitates understanding the effects of pressure and temperature variations on the mechanisms leading to induced seismicity.

Results show that thermal effects may be critical for geothermal stimulations. Overpressure affects the stress field, especially within the fracture zone, but it does not necessarily lead to unstable conditions. On the other hand, thermal perturbations cause an increase of the deviatoric stress in the cooled portion of the matrix, provoking an unstable condition. Thus, THM coupling describes processes that can play a key role in the triggering of induced seismicity. Furthermore, results show that the greatest thermal effects occur in the rock mass surrounding the fracture zone, which undergoes a significant reduction in stability.

It is worth noting that the overall process is very sensitive to the problem geometry (orientation of the fracture zone), stiffness parameters, stress state regime and confinement conditions. When the greatest confining stress acts normal to the fractures, thermal effects dominate and thermal stress reduction can trigger induced seismic events.

Acknowledgements

The work presented in this paper was funded by Geo-Energie Suisse AG.

S. De Simone wishes to acknowledge the financial support received from the AGAUR (Generalitat de Catalunya) through the "grant for universities and research centers for the recruitment of new research personnel (FI-DGR 2012)".

References

Baisch, S., Vörös, R., Rothert, E., Stang, H., Jung, R., Schellschmidt, R., 2010. A numerical model for fluid injection induced seismicity at Soultz-sous-Forêts. Int. J. Rock Mech. Min. Sci. 47, 405–413.

Baria, R., Michelet, S., Baumgärtner, J., Dyer, B., Nicholls, J., Hettkamp, T., Teza, D., Soma, N., Asanuma, H., Garnish, J., Megel, T., 2005. Creation and mapping of 5000 m deep HDR/HFR reservoir to produce electricity. In: Proceedings of the World Geothermal Congress 2005, Antalya, Turkey, Paper 1627, 8pp.

Barton, N., Bandis, S., Bakhtar, K., 1985. Strength, deformation and conductivity coupling of rock joints. Int. J. Rock Mech. Min. Sci. Geomech. Abstracts 22 (3), 121–140.

Bruel, D., 2002. Impact of induced thermal stresses during circulation tests in an engineered fractured geothermal reservoir; example of the Soultz-sous-Forets European hot fractured rock geothermal project, Rhine Graben, France. Oil Gas Sci. Technol. Rev. IFP 57, 459–470.

Byerlee, J., 1978. Friction of rocks. Pure Appl. Geophys. 116 (4), 615–626.

Cappa, F., Rutqvist, J., 2011. Modeling of coupled deformation and permeability evolution during fault reactivation induced by deep underground injection of CO_2. Int. J. Greenhouse Gas Control 5 (2), 336–346.

Cornet, F.H., Helm, J., Poitrenaud, H., Etchecopar, A., 1997. Seismic and aseismic slips induced by large-scale fluid injections. Pure Appl. Geophys. 150 (3), 563–583.

Delleur, J.W., (Ed. 1999). The handbook of groundwater engineering. CRC.

Engelder, T., Fischer, M.P., 1994. Influence of poroelastic behavior on the magnitude of minimum horizontal stress, Sh, in overpressured parts of sedimentary basins. Geology 22 (10), 949–952.

Evans, K.F., Moriya, H., Niitsuma, H., Jones, R.H., Phillips, W.S., Genter, A., Sausse, J., Jung, R., Baria, R., 2005. Microseismicity and permeability enhancement of hydrogeologic structures during massive fluid injections into granite at 3 km depth at the Soultz HDR site. Geophys. J. Int. 160, 389–412.

Evans, K.F., Zappone, A., Kraft, T., Deichmann, N., Moia, F., 2012. A survey of the induced seismic responses to fluid injection in geothermal and CO_2 reservoirs in Europe. Geothermics 41, 30–54.

Faulkner, D.R., Mitchell, T.M., Healy, D., Heap, M.J., 2006. Slip on 'weak' faults by the rotation of regional stress in the fracture damage zone. Nature 444, 922–925.

Ferronato, M., Gambolati, G., Janna, C., Teatini, P., 2008. Numerical modelling of regional faults in land subsidence prediction above gas/oil reservoirs. Int. J. Numer. Anal. Meth. Geomech. 32, 633–657.

Ghassemi, A., 2012. A review of some rock mechanics issues in geothermal reservoir development. Geotech. Geol. Eng., 1–18.

Ghassemi, A., Zhou, X., 2011. A three-dimensional thermo-poroelastic model for fracture response to injection/extraction in enhanced geothermal systems. Geothermics 40 (1), 39–49.

Ghassemi, A., Tarasovs, S., Cheng, A.H.-D., 2007. A 3-D study of the effects of thermomechanical loads on fracture slip in enhanced geothermal reservoirs. Int. J. Rock Mech. Min. Sci. 44, 1132–1148.

Ghassemi, A., Nygren, A., Cheng, A., 2008. Effects of heat extraction on fracture aperture: a poro-thermoelastic analysis. Geothermics 37 (5), 525–539.

Goodman, R.E., 1989. Introduction to Rock Mechanics, Wiley, New York.

Gudmundsson, A., 2004. Effects of Young's modulus on fault displacement. C.R. Geosci. 336 (1), 85–92.

Häring, M.O., Schanz, U., Ladner, F., Dyer, B.C., 2008. Characterization of the Basel 1 enhanced geothermal system. Geothermics 37, 469–495.

Hillis, R., 2000. Pore pressure/stress coupling and its implications for seismicity. Explor. Geophys. 31, 448–454.

Hoek, E. (2006 edition). Practical Rock Engineering. <www.rocscience.com>.

Jaeger, J.C., Cook, N.G.W., Zimmerman, R.W., 2007. Fundamentals of Rock Mechanics, fourth ed. Blackwell, Oxford.

Kohl, T., Evans, K.F., Hopkirk, R.J., Rybach, L., 1995. Coupled hydraulic, thermal and mechanical considerations for the simulation of hot dry rock reservoirs. Geothermics 24 (3), 345–359.

Kolditz, O., Clauser, C., 1998. Numerical simulation of flow and heat transfer in fractured crystalline rocks: application to the hot dry rock site in Rosemanowes (UK). Geothermics 27 (1), 1–23.

Majer, E.L., Baria, R., Stark, M., Oates, S., Bommer, J., Smith, B., Asanuma, H., 2007. Induced seismicity associated with enhanced geothermal systems. Geothermics 36, 185–222.

Mallikamas, W., Rajaram, H., 2005. On the anisotropy of the aperture correlation and effective transmissivity in fractures generated by sliding between identical self-affine surfaces. Geophys. Res. Lett. 32, L11401.

McDermott, C., Randriamanjatosoa, A.R.L., Tenzer, H., Kolditz, O., 2006. Simulation of heat extraction from crystalline rocks: the influence of coupled processes on differential reservoir cooling. Geothermics 35, 321–344.

McTigue, D.F., 1986. Thermoelastic response of fluid-saturated porous rock. J. Geophys. Res. 91 (B9), 9533–9542.

Morris, A., Ferrill, D.A., Henderson, D.B., 1996. Slip-tendency analysis and fault reactivation. Geology 24 (3), 275–278.

Mossop, A., Segall, P., 1997. Subsidence at the Geysers geothermal field, N. California from a comparison of GPS and leveling surveys. Geophys. Res. Lett. 24, 1839–1842.

National Research Council, 2012. Induced Seismicity Potential in Energy Technologies. The National Academies Press, Washington, DC, p. 1.

Olivella, S., Carrera, J., Gens, A., Alonso, E.E., 1994. Non-isothermal multiphase flow of brine and gas through saline media. Transp. Porous Media 15, 271–293.

Olivella, S., Gens, A., Carrera, J., Alonso, E.E., 1996. Numerical formulation for a simulator (CODE_BRIGHT) for the coupled analysis of saline media. Eng. Comput. 13, 87–112.

Parotidis, M., Shapiro, S.A., Rothert, E., 2004. Back front of seismicity induced after termination of borehole fluid injection. Geophys. Res. Lett. 31, L02612.

Pearson, C., 1981. The relationship between microseismicity and high pore pressures during hydraulic stimulation experiments in low permeability granitic rocks. J. Geophys. Res. 86, 7855–7864.

Ripperger, J., Kästli, P., Fäh, D., Giardini, D., 2009. Ground motion and macroseismic intensities of a seismic event related to geothermal reservoir stimulation below the city of Basel – observations and modeling. Geophys. J. Int. 179, 1757–1771.

Rutqvist, J., Stephansson, O., 2003. The role of hydromechanical coupling in fractured rock engineering. Hydrogeol. J. 11 (1), 7–40.

Schultz, R.A., 1996. Relative scale and the strength and deformability of rock masses. J. Struct. Geol. 18 (9), 1139–1149.

Segall, P., Fitzgerald, S.D., 1998. A note on induced stress changes in hydrocarbon and geothermal reservoirs. Tectonophysics 289, 117–128.

Segall, P., Grasso, J.-R., Mossop, A., 1994. Poroelastic stressing and induced seismicity near the Lacq gas field, southwestern France. J. Geophys. Res. 99 (B8), 15423–15438.

Shapiro, S.A., Audigane, P., Royer, J.J., 1999. Large-scale in situ permeability tensor of rocks from induced seismicity. Geophys. J. Int. 137, 207–213.

Shapiro, S.A., Patzig, R., Rothert, E., Rindschwentner, J., 2003. Triggering of seismicity by pore-pressure perturbations: permeability-related signatures of the phenomenon. Pure Appl. Geophys. 160, 1051–1066.

Streit, J.E., Hillis, R.R., 2004. Estimating fault stability and sustainable fluid pressures for underground storage of CO_2 in porous rock. Energy 29 (9), 1445–1456.

Vilarrasa, V., Bolster, D., Olivella, S., Carrera, J., 2010. Coupled hydromechanical modeling of CO_2 sequestration in deep saline aquifers. Int. J. Greenhouse Gas Control 4 (6), 910–919.

Yeo, I.W., de Freitas, M.H., Zimmerman, R.W., 1998. Effect of shear displacement on the aperture and permeability of a rock fracture. Int. J. Rock Mech. Min. Sci. 35 (8), 1051–1070.

Zimmerman, R.W., 2000. Coupling in poroelasticity and thermoelasticity. Int. J. Rock Mech. Min. Sci. 37 (1–2, 1), 79–87.

Zoback, D., 2007. Reservoir Geomechanics. Cambridge University Press, 504p (ISBN: 0521770696).